HHS Public Access

Author manuscript

Clin Biomech (Bristol, Avon). Author manuscript; available in PMC 2024 July 01.

Published in final edited form as:

Clin Biomech (Bristol, Avon). 2023 July ; 107: 106007. doi:10.1016/j.clinbiomech.2023.106007.

Assessing carpal kinematics following scapholunate interosseous ligament injury *ex vivo* using four-dimensional dynamic computed tomography

Taylor P. Trentadue, B.S.[a,b,c], **Cesar Lopez, M.S.**[a], **Ryan E. Breighner, Ph.D.**[d], **Mohsen Akbari-Shandiz, Ph.D.**[a,1], **Kai-Nan An, Ph.D.**[a], **Shuai Leng, Ph.D.**[e,f], **David R. Holmes III, Ph.D.**[f,g], **Steven L. Moran, M.D.**[h], **Sanjeev Kakar, M.D.**[h], **Jay Smith, M.D.**[i,2], **Andrew Thoreson, M.S.**[a], **Kristin D. Zhao, Ph.D.**[a,f,i,*]

[a]Assistive and Restorative Technology Laboratory, Rehabilitation Medicine Research Center, Department of Physical Medicine and Rehabilitation, Mayo Clinic, Rochester, MN

[b]Mayo Clinic Medical Scientist Training Program, Mayo Clinic, Rochester, MN

[c]Biomedical Engineering and Physiology Graduate Program, Mayo Clinic Graduate School of Biomedical Sciences, Mayo Clinic, Rochester, MN, USA

[d]Department of Radiology and Imaging, Hospital for Special Surgery, New York, NY

[e]CT Clinical Innovation Center, Department of Radiology, Mayo Clinic, Rochester, MN

[f]Department of Physiology and Biomedical Engineering, Mayo Clinic, Rochester, MN

[g]Biomedical Imaging Resource, Mayo Clinic College of Medicine, Mayo Clinic, Rochester, MN

[h]Department of Orthopedic Surgery, Division of Hand Surgery, Mayo Clinic, Rochester, MN

[i]Department of Physical Medicine and Rehabilitation, Mayo Clinic, Rochester, MN

[*]**Corresponding author** Kristin D. Zhao, Ph.D., Assistive and Restorative Technology Laboratory and Department of Physiology and Biomedical Engineering, Mayo Clinic, Rochester, Minnesota, USA, 200 First St. SW, Rochester, MN 55905, zhao.kristin@mayo.edu.
Mohsen Akbari-Shandiz, Ph.D., Assistive and Restorative Technology Laboratory, Mayo Clinic, Rochester, Minnesota, USA, 200 First St. SW, Rochester, MN 55905, moaksh@gmail.com
Ryan E. Breighner, Ph.D., Department of Radiology and Imaging, Hospital for Special Surgery, New York, New York, USA, 535 E 70th St., New York, NY 10021, breighnerr@hss.edu
David R. Holmes III, Ph.D., Biomedical Imaging Resource and Department of Physiology and Biomedical Engineering, Mayo Clinic, Rochester, Minnesota, USA, 200 First St. SW, Rochester, MN 55905, holmes.david3@mayo.edu
Sanjeev Kakar, M.D., Department of Orthopedic Surgery, Mayo Clinic, Rochester, Minnesota, USA, 200 First St. SW, Rochester, MN 55905, kakar.sanjeev@mayo.edu
Shuai Leng, Ph.D., Computed Tomography Clinical Innovation Center, Mayo Clinic, Rochester, Minnesota, USA, 200 First St. SW, Rochester, MN 55905, leng.shuai@mayo.edu
Cesar Lopez, M.S., Assistive and Restorative Technology Laboratory, Mayo Clinic, Rochester, Minnesota, USA, 200 First St. SW, Rochester, MN 55905, lopez.cesar@mayo.edu
Steven L. Moran, M.D., Department of Orthopedic Surgery, Mayo Clinic, Rochester, Minnesota, USA, 200 First St. SW, Rochester, MN 55905, moran.steven@mayo.edu
Jay Smith, M.D., Department of Physical Medicine and Rehabilitation, Mayo Clinic, Rochester, Minnesota, USA, 200 First St. SW, Rochester, MN 55905, jsmith@sonexhealth.com
Andrew R. Thoreson, M.S., Assistive and Restorative Technology Laboratory, Mayo Clinic, Rochester, Minnesota, USA, 200 First St. SW, Rochester, MN 55905, thoreson.andrew@mayo.edu
Taylor P. Trentadue, B.S., Assistive and Restorative Technology Laboratory, Mayo Clinic Medical Scientist Training Program, and Mayo Clinic Graduate Program in Biomedical Engineering and Physiology, Mayo Clinic, Rochester, Minnesota, USA, 200 First St. SW, Rochester, MN 55905, trentadue.taylor@mayo.edu
[1],present address: Koh Young Research America, San Diego, California, USA, 10920 Via Frontera, San Diego, CA 92127
[2],present address: Sonex Health, Inc., Eagan, Minnesota, USA, 950 Blue Gentian Road, #200, Eagan, MN 55121

Abstract

Background: Scapholunate interosseous ligament injuries are prevalent and often challenging to diagnose radiographically. Four-dimensional CT allows visualization of carpal bones during motion. We present a cadaveric model of sequential ligamentous sectionings ("injuries") to quantify their effects on interosseous proximities at the radioscaphoid joint and scapholunate interval. We hypothesized that injury, wrist position, and their interaction affect carpal arthrokinematics.

Methods: Eight cadaveric wrists were moved through flexion-extension and radioulnar deviation after injuries. Dynamic CT images of each motion were acquired in each injury condition using a second-generation dual-source CT scanner. Carpal osteokinematics were used to calculate arthrokinematic interosseous proximity distributions during motion. Median interosseous proximities were normalized and categorized by wrist position. Linear mixed-effects models and marginal means tests were used to compare distributions of median interosseous proximities.

Findings: The effect of wrist position was significant for both flexion-extension and radioulnar deviation at the radioscaphoid joint; the effect of injury was significant for flexion-extension at the scapholunate interval; and the effect of their interaction was significant for radioulnar deviation at the scapholunate interval. Across wrist positions, radioscaphoid median interosseous proximities were less able to distinguish injury conditions versus scapholunate proximities. Median interosseous proximities at the scapholunate interval are majoritively able to detect differences between less (Geissler I-III) versus more (Geissler IV) severe injuries when the wrist is flexed, extended, and ulnarly-deviated.

Interpretation: Dynamic CT enhances our understanding of carpal arthrokinematics in a cadaveric model of SLIL injury. Scapholunate median interosseous proximities in flexion, extension, and ulnar deviation best demonstrate ligamentous integrity.

Keywords

arthrokinematics; four-dimensional computed tomography (4DCT); radioscaphoid; scapholunate; scapholunate interosseous ligament (SLIL) injuries; wrist biomechanics

1. Introduction

The wrist is a complex joint comprised of eight carpal bones, with the proximal carpal row articulating with the radius (Rainbow et al., 2016). Ligaments—along with the osseous architecture—stabilize these bones, contribute to carpal stability, and serve as motion constraints (Berger, 2001; Kauer, 1980; Rainbow et al., 2016). Within the proximal carpal row, the scaphoid and lunate are joined by the scapholunate (SL) interosseous ligaments (SLIL) (Kauer, 1980; Kitay and Wolfe, 2012).

SLIL integrity contributes to normal SL motion (Kitay and Wolfe, 2012; Ruby et al., 1987; Short et al., 1995). Primary SL interval stabilizers include the intrinsic interosseous ligaments—comprised of anatomically-, functionally- and histologically-distinct volar, membranous, and dorsal components (Berger, 1996; Berger et al., 1999)—as well as secondary ligaments external to the SL interval (Berger, 1996; Berger et al., 1999; Kauer,

1980; Lee and Elfar, 2015; Linscheid et al., 1983; Mitsuyasu et al., 2004; Shahabpour et al., 2015; Viegas et al., 1999). The volar, or palmar, SLIL (VSL) contributes to rotational stability at the SL interval (Kitay and Wolfe, 2012). The membranous, or proximal, SLIL (MSL) has been shown to offer variable motion constraints in combination with other ligaments but provides minimal independent stability (Berger et al., 1999). The thicker dorsal SLIL (DSL) (Berger, 1996; Kauer, 1980) is thought to have the greatest contributions to scapholunate stability (Berger, 1996, 2001; Berger et al., 1999; Ruby et al., 1987; Short et al., 1995; Viegas et al., 1999). The palmar radioscaphocapitate (RSC) ligament acts as a secondary motion constraint at the SL interval (Short et al., 2002). The long radiolunate ligament (LRL), a portion of the volar radiocarpal joint capsule, is considered a critical lunate stabilizer (Badida et al., 2021; Berger, 1997; Sandow et al., 2014).

SLIL damage is a prevalent cause of wrist injury. SL instability occurs when the SL interval is damaged and unable to withstand applied load (Kitay and Wolfe, 2012; Rainbow et al., 2016). Clinically, this patient population presents with tenderness over the dorsoradial wrist, decreased grip strength, and a clicking or clunking sensation related to scaphoid displacement (Konopka and Chim, 2018). Patients may experience pain with wrist extension and radial deviation (Lee and Elfar, 2015). When untreated, SL instability may progress to the SL advanced collapse (SLAC) wrist pattern (McLean and Taylor, 2019; Watson et al., 1997), a major contributor to radiocarpal and midcarpal joint osteoarthritis (Watson and Ballet, 1984).

Injury to specific ligamentous portions is associated with more advanced SLIL injuries as categorized by Geissler grade (Geissler and Freeland, 1999; Lee and Elfar, 2015), which may be related to depth-related increases in tear thickness (Berger, 1996). In particular, the distinction between Geissler grades III and IV involves the completeness of the SLIL tear; in grade III, at least a portion of the DSL remains intact, whereas grade IV injuries represent a complete transection of the interosseous ligament complex (Geissler, 2013; Geissler and Freeland, 1999). Given the biomechanical and clinical relevance of the DSL, SLIL injuries can be broadly classified into less severe—intrinsic ligamentous injuries sparing the dorsal component—and more severe—including the DSL and extrinsic ligaments (Berger, 1996, 1997, 2001; Berger et al., 1999; Ruby et al., 1987; Short et al., 1995; Viegas et al., 1999).

The clinical and radiographic diagnosis of SL injury remains challenging, particularly in less severe injuries wherein functional and biomechanical changes are most discernible during dynamic activities (Short et al., 2002). Traditional static imaging—such as radiographs, CT, or MRI—may not optimally capture these injuries, as they often manifest during motion or wrist-loading activities (Meade et al., 1990; Rainbow et al., 2016; Short et al., 2002). Radiocarpal arthroscopy is commonly used in SLIL injury intraoperative diagnosis or repair, but it is an invasive procedure with limited preoperative applicability (Bakker et al., 2022; Mathoulin and Gras, 2020; Mathoulin et al., 2021).

Given these limitations, dynamic imaging modalities have been explored in the diagnosis of SL injury (Konopka and Chim, 2018; Schmid et al., 2005; Sulkers et al., 2014). Four-dimensional computed tomography (4DCT), which involves three-dimensional CT scanning over a defined time interval, such as a motion cycle, acquires images with high spatial

and temporal resolution. Previous studies have demonstrated that SL injuries and associated biomechanical outcomes can be detected using 4DCT (Brinkhorst et al., 2021b; Carr et al., 2019; de Roo et al., 2019; Kakar et al., 2016; Leng et al., 2011; Mat Jais and Tay, 2017; Robinson et al., 2021; White et al., 2019). Further, proof-of-concept studies have demonstrated the feasibility of 4DCT in cadaveric models of wrist motion (Tay et al., 2007).

The current study uses 4DCT to assess changes in interosseous proximities in a cadaveric model of ultrasound-guided SL ligamentous integrity sectionings, simulating progressive injury severity. This study seeks to further understand the contributions of intrinsic and extrinsic ligaments to scapholunate and radiocarpal stability using interosseous proximity distributions as a marker of arthrokinematics. As arthrokinematics are related to pressure distributed across a joint, interosseous proximities reflect how ligamentous injuries manifest at articular surfaces.

This study seeks to understand how the magnitude of radioscaphoid interosseous proximities and scapholunate diastasis is associated with specific SL ligamentous damage and whether there are position-related patterns. By using the intact wrist as a comparator, the cadaveric model readily allows interpretation of the effects of specific injuries on carpal arthrokinematics. This addresses the diagnostic gap in developing a noninvasive imaging biomarker for SLIL injury.

We hypothesize that, for both motion types included in this study (flexion-extension and radioulnar deviation) and for both joints of interest (radioscaphoid and scapholunate), (1) interosseous proximities during motion vary with ligamentous sectioning condition (injury) and wrist position relative to neutral (position) independently; (2) interosseous proximities vary with the interaction between injury and position; and (3) interosseous proximities exhibit interspecimen variability; this analysis will estimate the amount of variation. Further, we hypothesize that post-hoc comparisons between injury conditions will reveal significant differences in interosseous proximities between sequential injuries across wrist positions: we hypothesize that increasingly severe injuries will have decreased radioscaphoid and increased scapholunate interosseous proximities.

2. Materials and Methods

2.1 Research subjects

This study was approved by our institution’s biospecimens subcommittee (IRB #17-001279). Data were collected from fresh-frozen cadaveric upper extremity specimens procured through the institutional anatomic bequest program, excluding those with history of wrist pathology or evidence of bone trauma, fractures, significant arthritic change, or previous wrist surgery. Specimens were amputated at the mid-humerus while frozen. An age- and sex-matched sample (n=8 specimens; 50% female) was used. The mean (standard deviation [SD]) age of cadavers at the time of death was 71.8 (6.9) years, ranging from 61 to 82 years.

2.2 Data collection methods

2.2.1 Image acquisition—A second-generation dual-source CT scanner (SOMATOM Definition Flash, Siemens Healthcare, Germany) was used to acquire neutral-static 3DCT and dynamic 4DCT images of all specimens. In this scanner, two independent but identical X-ray tubes are configured on a rotating gantry at approximately 90-degree offset with respective detector arrays (38.4 mm in the proximal-distal direction) opposing each tube.

Static 3DCT images of the cadaveric wrist and distal forearm were acquired using a routine wrist CT scan protocol (120 kV, 200 effective mAs, gantry rotation time: 1 second). Dynamic CT data were acquired using a retrospective ECG-gated, dual-source cardiac CT protocol with sequential mode. In four-dimensional cardiac image protocols, CT volumes are acquired at evenly-spaced temporal intervals across the cardiac cycle. The ECG simulator was used to satisfy the existing cardiac imaging base protocol and to create a dynamic acquisition interval permitting slow, periodic gross wrist motion (Leng et al., 2011; Tay et al., 2008). The scan was conducted over a two-second period as triggered by an external ECG simulator set to 30 beats per minute (Tay et al., 2007). With retrospective ECG gating, one CT image volume was captured at 5% increments from 10% to 95% of the simulated cardiac cycle; this yielded eighteen CT volumes evenly temporally distributed (75 ms) across the motion cycle. The resulting voxel dimension was $0.234 \times 0.234 \times 0.600\ mm^3$. Dynamic images were acquired without table translation using a tube potential of 120 kV and an effective dose of 200 mAs, corresponding to a $CTDI_{vol}$ of 110 mGy per 4DCT scan (Leng et al., 2011). Data were projected using iterative reconstruction with a sharp kernel (I70f\3, SAFIRE, Siemens Healthineers, Forchheim, Germany).

During analysis, image volumes were resampled to isometric voxels with standard dimensions of $0.234 \times 0.234 \times 0.234\ mm^3$. Isotropic voxels were used to maintain consistent spatial resolution in the transverse and longitudinal dimensions as bones translated and rotated through orientations oblique to the transverse plane during wrist motion (Jaffe et al., 2006). To achieve isotropic scaling, standard trilinear interpolation was used (Thévenaz et al., 2008).

2.2.2 Cadaveric preparation and motion simulation—A custom electronic-pneumatic motion simulator was used to drive the wrists through a full motion cycle during the dynamic scanning interval (Zhao et al., 2015). The device consisted of a stepper motor-driven linear actuator to drive oscillatory hand motion with pneumatic cylinders applying force to tendons to simulate coordinating muscle load, with actions coordinated by a microcontroller (DMX-UMD-23, Arcus Technology, The Colony, TX, USA).

The proximal ulna and radius were secured to the simulator frame using two threaded Kirschner wires. The proximal ends of the flexor carpi radialis (FCR), flexor carpi ulnaris (FCU), extensor carpi ulnaris (ECU), and extensor carpi radialis brevis and longus (ECRB/ECRL) tendons were separated and each joined to one of four separate Dacron cords. Each cord was connected to a pneumatic cylinder mounted on the frame. Activation of the pneumatic cylinders was coordinated with wrist motion by loading flexor or extensor muscle tendons with 10 N (8.4 psi) of force when the linear actuator deviated the hand in the corresponding direction. Flexion was accompanied by the FCR and FCU loads; extension

with the ECRL and ECU loads; radial deviation with the FCR and ECRL loads; and ulnar deviation with the FCU and ECU loads. Wrists were moved through motion arcs at 30° per second. A metal clamp was used to secure the hand, near the level of the distal metacarpals, to a stage that allowed free motion along the longitudinal axis and was driven by a stepper motor along the perpendicular axis. The motion simulator was programmed to cyclically drive wrist motion between 45° flexion and 45° extension or between 30° radial deviation and 45° ulnar deviation at a rate of 0.5 Hz (Figure 1a). Wrists were cycled at least five times between each ligament sectioning and 4DCT acquisition.

Dynamic datasets were obtained first with specimens intact and then following each of five scapholunate interosseous ligament or extrinsic ligamentous sectionings conducted by a physiatrist under ultrasound guidance using a 3.0 mm V-shaped meniscotome (ACUFEX V-shaped meniscotome, Smith & Nephew, Inc., Andover, MA, USA). In validation pilot testing, ligament injuries were made under ultrasound guidance and confirmed with arthroscopy (Figure 1a, 1b, 1c). Separate flexion-extension and radioulnar deviation arcs were acquired. Ligament sectionings for each specimen followed the same sequence: all ligaments intact with subsequent disruption of the VSL, MSL, DSL, RSC, and LRL ligaments (Berger, 1996; Berger et al., 1999; Kitay and Wolfe, 2012; Lee and Elfar, 2015; Linscheid and Dobyns, 1992). A photograph demonstrating experimental set-up and execution is presented in the CT imaging suite (Figure 2).

2.3 Image processing

Complete descriptions of techniques used for 4DCT image analysis have been elaborated previously (Kakar et al., 2016; Leng et al., 2011; Trentadue et al., 2023; Zhao et al., 2015). After image acquisition, neutral-static 3DCT volumes were segmented to yield bone surface mesh models for the radius, scaphoid, lunate, and capitate. A custom surface registration algorithm developed using MATLAB (versions R2019a – R2022a, Natick, MA, USA) was used to co-register static to dynamic bone volumes at each timepoint in the 4DCT acquisition. Initial coarse alignment between the segmented static bone (“source”) and its corresponding position in the dynamic CT image volume (“target”) was performed using Söderkvist’s method (singular value decomposition) on manually-selected point landmarks (Söderkvist and Wedin, 1993). Precise alignment was conducted using a Nelder-Mead simplex optimization algorithm, which maximized normalized cross-correlation of surface intensity by adjusting motion parameters of each of six degrees-of-freedom. Optimization continued until either a defined threshold or iteration limit was reached. Subsequent frames were processed using automated optimization and intensity-based registration using the osteokinematics from the previous image volume as an initial input (Akbari-Shandiz et al., 2019; Breighner et al., 2013, 2016; Nelder and Mead, 1965).

The registration processed yielded osteokinematics, or six degree-of-freedom kinematics of each bone, in an imaging-based coordinate system. Neutral position was defined as the image volume wherein the radiocapitate angle was closest to 0° in the dominant plane of motion. Hand position in the motion cycle relative to neutral—wrist flexed, extended, radially-deviated, or ulnarly-deviated—was visually inspected and measured as the longitudinal axes between the radius and capitate in Mayo Clinic Analyze (Mayo

Foundation for Medical Education and Research, Rochester, MN, USA) on each dynamic CT volume. Three-dimensional triangular surface meshes were used to establish a radius-based coordinate system (Hillstrom et al., 2014; Wu et al., 2005).

Osteokinematics at each time point were used to define bone positions and calculate arthrokinematics. Arthrokinematics, or the interaction between adjacent bones at articulating surfaces, were quantified using interosseous proximities. Interosseous proximities were defined as the nearest mesh-vertex distances between all vertices within distance thresholds (radioscaphoid: 2.5 mm; scapholunate: 5.0 mm) and surface-normal angular thresholds (60°) between bone pairs were calculated. Interosseous proximity maps were generated to graphically represent the distribution of interosseous proximities on adjacent bone surface mesh vertices.

As some data sets contained more than one complete motion cycle and others an incomplete motion cycle, due to scanner acquisition period differences, data were truncated to include the longest continuous motion arc. All median proximities were normalized by dividing the measured proximity in each condition by the median proximity of the intact wrist in the neutral position. Wrist position designation, relative to neutral, was used to compute an aggregate median of all median interosseous proximities categorized as having the same relative position.

2.4 Statistical analysis

Linear mixed-effects models were conducted to evaluate the normalized interosseous proximities for each combination of joint (radioscaphoid and scapholunate) and wrist motion (flexion-extension and radioulnar deviation). As repeated measures were acquired, this technique accounted for correlated measurements within and across ligament sectionings, timepoints within a motion cycle, and cadavers. Linear mixed modeling analyses were conducted in MATLAB (R2022a, Natick, MA, USA). Fixed effects included (1) ligamentous sectioning condition (injury), (2) wrist position relative to neutral (position), and (3) interaction between injury and position (fixed effects coefficients = 12). Random effects included (1) cadaver and the interactions between (2) cadaver and injury and (3) cadaver and position (random effects coefficients = 72). The model specification was as follows: Median ~ Injury * Position + (1|Cadaver) + (1|Cadaver:Injury) + (1|Cadaver:Position). Cadaver —as well as its interactions with injury and position—was included as a random effect because the intrinsic variability in mechanics of each unique specimen has some impact on interosseous proximity patterns. Analyses of variance (ANOVA) for linear mixed-effects models were conducted for each fixed-effects term in the linear mixed-effects models. Post-hoc analyses included pairwise marginal means by injury and position at both joints during both motions. To summarize patterns, “majoritively” will be used to describe whether at least eight of nine possible pairwise combinations between less severe (PRE, VSL, MSL) and more severe (DSL, RSC, LRL) injuries achieved statistical significance in post-hoc marginal means tests in each wrist position.

3. Results

Demonstrative interosseous proximity maps are presented from one representative cadaver at the radioscaphoid joint and scapholunate interval across ligament integrity conditions at extrema of motions for flexion-extension (Figure 3) and radioulnar deviation (Figure 4).

Median (25^{th} – 75^{th} percentile) normalized interosseous proximities by joint and relative wrist position are presented (Supplementary Table 1) at the radioscaphoid joint (Figure 5) and the scapholunate interval (Figure 6).

Results from the linear mixed-effects models and ANOVA marginal tests at the radioscaphoid joint reveal that position is significant in both flexion-extension and radioulnar deviation (Supplementary Table 2). Results from the linear mixed-effects models and ANOVA marginal tests at the scapholunate interval reveal that injury is significant in flexion-extension and the interaction between injury and position is significant for radioulnar deviation (Supplementary Table 3).

At the radioscaphoid joint, flexed wrists can be distinguished from extended wrists (significant marginal means: 11/36 combinations) (Supplementary Table 4, Supplementary Table 6). At the scapholunate interval, flexed wrists can be distinguished from extended wrists (16/36 combinations). Less severe and more severe injuries are majoritively distinguishable in both wrist flexion (9/9 combinations) and wrist extension (8/9 combinations) (Supplementary Table 4, Supplementary Table 6).

At the radioscaphoid joint, radially-deviated wrists are distinguishable from ulnarly-deviated wrists (35/36 combinations); however, specific ligamentous integrity-related patterns cannot be detected (Supplementary Table 5, Supplementary Table 6). At the scapholunate interval, radially-deviated wrists are distinguishable from ulnarly-deviated wrists (18/36 combinations), with less severe injuries distinguishable from more severe injuries in ulnar deviation (9/9 combinations) (Supplementary Table 5, Supplementary Table 6).

Across wrist positions, median radioscaphoid interosseous proximities are generally indistinguishable between ligamentous integrity conditions; the only statistically-significant difference in percent neutral intact median proximity is between MSL and LRL in radial deviation (99.1% versus 95.4%, respectively) (Figure 5, Supplementary Table 6).

Median interosseous proximities at the scapholunate interval majoritively separate less severe and more severe injury groups when the wrist is flexed (9/9 comparisons), extended (8/9 comparisons), and ulnarly-deviated (9/9 comparisons) (Figure 6, Supplementary Table 6).

In flexion, percent neutral intact median proximity of PRE (median 103.2%) is statistically less than each DSL, RSC, and LRL (116.9%, 118.4%, and 120.3%, respectively); VSL (110.0%) is statistically less than each DSL, RSC, and LRL; and MSL (114.0%) is statistically less than RSC and LRL.

In extension, percent neutral intact median proximity of PRE (108.6%) is statistically less than each DSL, RSC, and LRL (113.8%, 116.2%, and 118.9%, respectively); VSL (106.6%) is statistically less than each DSL, RSC, and LRL; and MSL (106.2%) is statistically less than DSL, RSC, and LRL.

In ulnar deviation, percent neutral intact median proximity of PRE (111.5%) is statistically less than each DSL, RSC, and LRL (116.6%, 115.9%, and 125.9%, respectively); VSL (113.2%) is statistically less than each DSL, RSC, and LRL; MSL (112.3%) is statistically less than DSL, RSC, and LRL; and RSC is significantly less than LRL. Both extension and ulnar deviation completely separate less severe and more severe injury groups. No statistically significant differences were found in radial deviation.

4. Discussion

SLIL injuries are a common cause of impaired wrist function that, when left untreated, may progress to SLAC wrist and radiocarpal osteoarthritis (Kitay and Wolfe, 2012; McLean and Taylor, 2019; Rainbow et al., 2016; Watson and Ballet, 1984; Watson et al., 1997). Leveraging advancements in 4DCT technology and analysis, this study reports incremental changes in scapholunate interval arthrokinematics following progressive SLIL sectioning, simulating incrementally worsening ligamentous integrity conditions by quantifying interosseous proximities at the radioscaphoid joint and scapholunate interval during wrist motions. This builds upon previous literature, which has detected minor kinematic alterations following SLIL sectionings (Badida et al., 2021; Short et al., 2002).

The anatomy of the SLIL constrains relative scaphoid and lunate motion during functional tasks involving the wrist (Kauer, 1980). The thicker dorsal SLIL (DSL) (Berger, 1996; Kauer, 1980) is thought to have the greatest contributions to carpal stability (Berger, 1996, 2001; Berger et al., 1999; Ruby et al., 1987; Short et al., 1995; Viegas et al., 1999). The current data demonstrate that greatest changes in interosseous proximities at the scapholunate interval occur after injury to the DSL, during both flexion-extension and radioulnar deviation. This is in line with a previous study of wrist kinematics *ex vivo*, which revealed that isolated DSL injury contributed to greater changes in motion than isolated VSL sectioning (Waters et al., 2016).

Previous studies have demonstrated that, in wrist flexion-extension, greatest radiocarpal joint motion can be appreciated as the wrist moves from neutral to extension (Rainbow et al., 2013; Rainbow et al., 2016). The current analyses reveal that wrist position is significant for both flexion-extension and radioulnar deviation at the radioscaphoid joint, indicating that median radioscaphoid interosseous proximities can distinguish when the wrist is flexed versus extended. The current data do not reveal a clear pattern of radioscaphoid interosseous proximity changes following injury. This may be due to the limited wrist cycling prior to 4DCT acquisition, as more motion cycles may be needed for viscoelastic ligamentous stretching to a steady state. Radiocarpal joint changes—including subsequent progression to SLAC wrist and radiocarpal OA—are longer-term, chronic implications of SLIL injury and may not be adequately captured in this cadaveric model (Watson and Ballet, 1984; Watson et al., 1997).

The geometry of the carpal bones contributes to their motion patterns. Both the scaphoid and the lunate are wedge-shaped in coronal section and have the tendency to separate during radioulnar deviation (Kauer, 1980). A previous study revealed that SLIL disruption changed scaphoid and lunate motion during flexion-extension but not during radioulnar deviation (Short et al., 2002). The current study reveals that injury is significant in distinguishing median interosseous proximities during flexion-extension and that the interaction between injury and position is significant during radioulnar deviation at the scapholunate interval.

Four-dimensional computed tomography permits calculation of both osteokinematics and arthrokinematics. Previous work has focused on elucidating carpal osteokinematics from quasi-dynamic and dynamic CT (Abe et al., 2018; Brinkhorst et al., 2021a, b; de Roo et al., 2019; Mat Jais and Tay, 2017; Padmore et al., 2019; Zhao et al., 2015). Osteokinematics may be dependent on manually-selected bone landmarks and landmark-based coordinate systems, wherein minor variations in landmark definitions may propagate errors. By calculating interactions across surfaces, landmark-related errors are mitigated. Further, whereas osteokinematics reflect patterns of bone centroids, arthrokinematics is associated with pressure across a joint. As a clinical correlate of scapholunate injury is SLAC pattern osteoarthritis, arthrokinematics and interosseous proximity maps may be better associated with osteoarthritis and provide richer information about articulating surface interactions (Robinson et al., 2021). Finally, ligamentous injury may result in subtle osteokinematic changes that are less detectable using standard kinematic outcomes (Robinson et al., 2021).

The current study reveals majoritive differences in scapholunate interosseous proximities between less severe (intact, VSL, and MSL) versus more severe (DSL, RSC, and LRL) injuries when the wrist is in flexion, extension, and ulnar deviation. Thus, these three positions may be compelling for injury detection within the context of a dynamic assessment.

4.1 Limitations

The findings of our study must be viewed in the context of its limitations. First, by using cadaveric models, we are unable to assess physiologic and pathophysiologic motion. While the SL interval receives stability from active muscular forces (Kauer, 1980; León-López et al., 2014), we cannot ascertain those contributions in our experimental model. A goal of our study is to be able to apply the findings from specific ligamentous injury *ex vivo* to *in vivo* patient cases.

Further, the current study included median interosseous proximities by wrist position relative to neutral and not as a function of gross wrist angle. However, due to factors such as pain and swelling after injury, patients may not be able to move through physiologic ranges of joint motion; this study demonstrates that differences are detectable across a range of wrist positions from neutral to the extrema of a given wrist position. Additionally, osteokinematic and arthrokinematic data were not interpolated, so the interosseous proximities were not determined at consistent wrist angles within and between participants. Only one 4DCT dataset in each motion and ligamentous integrity condition was collected per specimen; future work should address the intraspecimen variability within a given condition.

Given the limited sample size, the current study did not consider the contributions of specific lunate morphologies to carpal kinematics (Abe et al., 2018; Rhee and Moran, 2020). The cadavers have a mean (SD) age higher than the clinical population with SLIL injuries; while notable osteoarthritis was an exclusion criterion, these specimens may have some degree of scattered osteoarthritis within the carpus.

Wrists were cycled at minimum five times following injury. This relatively limited cycling prior to 4DCT acquisition may have been insufficient for the chronic sequelae of injury patterns, including SLAC wrist, to manifest at the radioscaphoid joint. The data from the study reflect a single ligamentous sectioning sequence, which limits the ability to understand contributions of individual ligaments (Badida et al., 2021). While validation pilot studies used arthroscopy to confirm ultrasound-guided injuries, arthroscopic confirmation of each ligament injury was not conducted in the full dataset.

Our study assessed flexion-extension and radioulnar deviation but not the dart-thrower's motion: while there is limited movement between the scaphoid and lunate in vivo (Leventhal et al., 2010) and global dart-thrower's motion is preserved following SLIL and LRL sectioning (Badida et al., 2021), it is possible that pathologic arthrokinematics develop following certain ligamentous injuries (Garcia-Elias et al., 2014; Rainbow et al., 2016).

4.2 Clinical applications

This study helps to inform our understanding of how sequential ligament injuries influence arthrokinematics at the radioscaphoid joint and scapholunate interval. This study demonstrates certain wrist positions—notably flexion, extension, and ulnar deviation—that accentuate interosseous proximity changes at the scapholunate interval following ligamentous injury and provides insight into the magnitude of change compared to an uninjured wrist. This cadaveric model provides a comparative dataset against which patient interosseous proximity data can be evaluated. While osteokinematics—and therefore arthrokinematics—from cadaveric experiments do not replicate *in vivo* dynamics, the arthrokinematic patterns derived from this cadaveric dataset be used to inform clinical injury diagnosis. Future studies will explore how cadaveric models of wrist ligamentous injuries may serve as predictive datasets for patient injury classification.

5. Conclusion

SLIL injuries are a major contributor to wrist dysfunction and have the potential to progress to radiocarpal osteoarthritis. This study provides foundational arthrokinematic data following sequential SLIL ligament compromise, the general patterns from which may influence the diagnosis of *in vivo* scapholunate interval injury.

Supplementary Material

Refer to Web version on PubMed Central for supplementary material.

Acknowledgements

This work was supported by the National Institutes of Health (NIH NIAMS R01 AR071338, NIH NIGMS T32 GM065841, and NIH NIAMS T32 AR056950). The authors thank Ryan Lennon, M.S., for statistical consultations and guidance. The authors thank Kalli Fautsch, B.A., B.S., for assistance with cadaveric data processing. The authors thank the Mayo Clinic Computed Tomography Clinical Innovation Center and the Mayo Clinic X-Ray Imaging Core Facility.

References

Abe S, Moritomo H, Oka K, Sugamoto K, Kasubuchi K, Murase T, Yoshikawa H, 2018. Three-dimensional kinematics of the lunate, hamate, capitate and triquetrum with type 1 or 2 lunate morphology. The Journal of hand surgery, European volume 43, 380–386. [PubMed: 29228850]

Akbari-Shandiz M, Breighner RE, Holmes DR III, Zhao KD, 2019. An interpolation method to evaluate impact of scapholunate ligament injuries on carpal bone kinematics in patients with unilateral injuries using 4DCT imaging, Orthopedic Research Society, Austin, TX, USA.

Badida R, Akhbari B, Vutescu E, Moore DC, Wolfe SW, Crisco JJ, 2021. The role of scapholunate interosseous, dorsal intercarpal, and radiolunate ligaments in wrist biomechanics. Journal of biomechanics 125, 110567. [PubMed: 34246909]

Bakker D, Kortlever JTP, Kraan GA, Mathijssen N, Colaris JW, Ring D, 2022. Treatment recommendations for suspected scapholunate ligament pathology. Journal of wrist surgery 11, 62–68. [PubMed: 35127266]

Berger RA, 1996. The gross and histologic anatomy of the scapholunate interosseous ligament. The Journal of hand surgery 21, 170–178. [PubMed: 8683042]

Berger RA, 1997. The ligaments of the wrist. A current overview of anatomy with considerations of their potential functions. Hand clinics 13, 63–82. [PubMed: 9048184]

Berger RA, 2001. The anatomy of the ligaments of the wrist and distal radioulnar joints. Clinical orthopaedics and related research, 32–40. [PubMed: 11210966]

Berger RA, Imeada T, Berglund L, An KN, 1999. Constraint and material properties of the subregions of the scapholunate interosseous ligament. The Journal of hand surgery 24, 953–962. [PubMed: 10509273]

Breighner R, Holmes DR 3rd, Leng S, An KN, McCollough C, Zhao K, 2013. 3D-3D Registration of partial capitate bones using spin-images. Proc SPIE Int Soc Opt Eng 8671.

Breighner R, Holmes DR 3rd, Leng S, An KN, McCollough C, Zhao K, 2016. Relative accuracy of spin-image-based registration of partial capitate bones in 4DCT of the wrist. Comput Methods Biomech Biomed Eng Imaging Vis 4, 360–367. [PubMed: 27722036]

Brinkhorst M, Foumani M, van Rosmalen J, Selles R, Hovius S, Strackee S, Streekstra G, 2021a. Four-dimensional CT analysis of carpal kinematics: An explorative study on the effect of sex and hand-dominance. Journal of biomechanics, 110870. [PubMed: 34838290]

Brinkhorst M, Foumani M, van Rosmalen J, Selles R, Hovius S, Strackee S, Streekstra G, 2021b. Quantifying in vivo scaphoid, lunate, and capitate kinematics using four-dimensional computed tomography. Skeletal radiology 50, 351–359. [PubMed: 32734373]

Carr R, MacLean S, Slavotinek J, Bain GI, 2019. Four-dimensional computed tomography scanning for dynamic wrist disorders: prospective analysis and recommendations for clinical utility. Journal of wrist surgery 8, 161–167. [PubMed: 30941259]

de Roo MGA, Muurling M, Dobbe JGG, Brinkhorst ME, Streekstra GJ, Strackee SD, 2019. A four-dimensional-CT study of in vivo scapholunate rotation axes: possible implications for scapholunate ligament reconstruction. The Journal of hand surgery, European volume 44, 479–487. [PubMed: 30813846]

Garcia-Elias M, Alomar Serrallach X, Monill Serra J, 2014. Dart-throwing motion in patients with scapholunate instability: a dynamic four-dimensional computed tomography study. The Journal of hand surgery, European volume 39, 346–352. [PubMed: 23571486]

Geissler WB, 2013. Arthroscopic management of scapholunate instability. Journal of wrist surgery 2, 129–135. [PubMed: 24436805]

Geissler WB, Freeland AE, 1999. Arthroscopic management of intra-articular distal radius fractures. Hand clinics 15, 455–465, viii. [PubMed: 10451821]

Hillstrom HJ, Garg R, Kraszewski A, Lenhoff M, Carter T, Backus SI, Wolff A, Syrkin G, Cheng R, Wolfe SW, 2014. Development of an anatomical wrist joint coordinate system to quantify motion during functional tasks. J Appl Biomech 30, 586–593. [PubMed: 24615208]

Jaffe TA, Nelson RC, Johnson GA, Lee ER, Yoshizumi TT, Lowry CR, Bullard AB, DeLong DM, Paulson EK, 2006. Optimization of multiplanar reformations from isotropic data sets acquired with 16–detector row helical CT scanner. Radiology 238, 292–299. [PubMed: 16373774]

Kakar S, Breighner RE, Leng S, McCollough CH, Moran SL, Berger RA, Zhao KD, 2016. The role of dynamic (4D) CT in the detection of scapholunate ligament injury. J Wrist Surg 5, 306–310. [PubMed: 27777822]

Kauer JM, 1980. Functional anatomy of the wrist. Clinical orthopaedics and related research, 9–20.

Kitay A, Wolfe SW, 2012. Scapholunate instability: current concepts in diagnosis and management. The Journal of hand surgery 37, 2175–2196. [PubMed: 23021178]

Konopka G, Chim H, 2018. Optimal management of scapholunate ligament injuries. Orthopedic research and reviews 10, 41–54. [PubMed: 30774459]

Lee DJ, Elfar JC, 2015. Carpal ligament injuries, pathomechanics, and classification. Hand clinics 31, 389–398. [PubMed: 26205700]

Leng S, Zhao K, Qu M, An KN, Berger R, McCollough CH, 2011. Dynamic CT technique for assessment of wrist joint instabilities. Med Phys 38 Suppl 1, S50. [PubMed: 21978117]

León-López MM, García-Elías M, Salvà-Coll G, Llusá-Perez M, Lluch-Bergadà A, 2014. [Muscular control of scapholunate instability. An experimental study]. Revista espanola de cirugia ortopedica y traumatologia 58, 11–18. [PubMed: 24360400]

Leventhal EL, Moore DC, Akelman E, Wolfe SW, Crisco JJ, 2010. Carpal and forearm kinematics during a simulated hammering task. The Journal of hand surgery 35, 1097–1104. [PubMed: 20610055]

Linscheid RL, Dobyns JH, 1992. Treatment of scapholunate dissociation. Rotatory subluxation of the scaphoid. Hand clinics 8, 645–652. [PubMed: 1460063]

Linscheid RL, Dobyns JH, Beckenbaugh RD, Cooney WP 3rd, Wood MB, 1983. Instability patterns of the wrist. The Journal of hand surgery 8, 682–686. [PubMed: 6630949]

Mat Jais IS, Tay SC, 2017. Kinematic analysis of the scaphoid using gated four-dimensional CT. Clin Radiol 72, 794.e791–794.e799.

Mathoulin C, Gras M, 2020. Role of wrist arthroscopy in scapholunate dissociation. Orthop Traumatol Surg Res 106, S89–s99. [PubMed: 31740161]

Mathoulin C, Merlini L, Taleb C, 2021. Scapholunate injuries: challenging existing dogmas in anatomy and surgical techniques. The Journal of hand surgery, European volume 46, 5–13. [PubMed: 32954904]

McLean A, Taylor F, 2019. Classifications in brief: Watson and Ballet classification of scapholunate advanced collapse wrist arthritis. Clinical orthopaedics and related research 477, 663–666. [PubMed: 30179931]

Meade TD, Schneider LH, Cherry K, 1990. Radiographic analysis of selective ligament sectioning at the carpal scaphoid: a cadaver study. The Journal of hand surgery 15, 855–862. [PubMed: 2269773]

Mitsuyasu H, Patterson RM, Shah MA, Buford WL, Iwamoto Y, Viegas SF, 2004. The role of the dorsal intercarpal ligament in dynamic and static scapholunate instability. The Journal of hand surgery 29, 279–288. [PubMed: 15043902]

Nelder JA, Mead R, 1965. A simplex method for function minimization. The Computer Journal 7, 308–313.

Padmore CE, Stoesser H, Langohr GDG, Johnson JA, Suh N, 2019. Carpal kinematics following sequential scapholunate ligament sectioning. Journal of wrist surgery 8, 124–131. [PubMed: 30941252]

Rainbow MJ, Kamal RN, Leventhal E, Akelman E, Moore DC, Wolfe SW, Crisco JJ, 2013. In vivo kinematics of the scaphoid, lunate, capitate, and third metacarpal in extreme wrist flexion and extension. The Journal of hand surgery 38, 278–288. [PubMed: 23266007]

Rainbow MJ, Wolff AL, Crisco JJ, Wolfe SW, 2016. Functional kinematics of the wrist. The Journal of hand surgery, European volume 41, 7–21. [PubMed: 26568538]

Rhee PC, Moran SL, 2020. The effect of lunate morphology in carpal disorders: review of the literature. Curr Rheumatol Rev 16, 184–188. [PubMed: 30887926]

Robinson SM, Straatman L, Lee TY, Suh N, Lalone E, 2021. Evaluation of four-dimensional computed tomography as a technique for quantifying carpal motion. J Biomech Eng.

Ruby LK, An KN, Linscheid RL, Cooney WP 3rd, Chao EY, 1987. The effect of scapholunate ligament section on scapholunate motion. The Journal of hand surgery 12, 767–771. [PubMed: 3655239]

Sandow MJ, Fisher TJ, Howard CQ, Papas S, 2014. Unifying model of carpal mechanics based on computationally derived isometric constraints and rules-based motion - the stable central column theory. The Journal of hand surgery, European volume 39, 353–363. [PubMed: 24072199]

Schmid MR, Schertler T, Pfirrmann CW, Saupe N, Manestar M, Wildermuth S, Weishaupt D, 2005. Interosseous ligament tears of the wrist: comparison of multi-detector row CT arthrography and MR imaging. Radiology 237, 1008–1013. [PubMed: 16304116]

Shahabpour M, Staelens B, Van Overstraeten L, De Maeseneer M, Boulet C, De Mey J, Scheerlinck T, 2015. Advanced imaging of the scapholunate ligamentous complex. Skeletal radiology 44, 1709–1725. [PubMed: 26219592]

Short WH, Werner FW, Fortino MD, Palmer AK, Mann KA, 1995. A dynamic biomechanical study of scapholunate ligament sectioning. The Journal of hand surgery 20, 986–999. [PubMed: 8583072]

Short WH, Werner FW, Green JK, Masaoka S, 2002. Biomechanical evaluation of ligamentous stabilizers of the scaphoid and lunate. The Journal of hand surgery 27, 991–1002. [PubMed: 12457349]

Söderkvist I, Wedin PA, 1993. Determining the movements of the skeleton using well-configured markers. Journal of biomechanics 26, 1473–1477. [PubMed: 8308052]

Sulkers GS, Schep NW, Maas M, van der Horst CM, Goslings JC, Strackee SD, 2014. The diagnostic accuracy of wrist cineradiography in diagnosing scapholunate dissociation. The Journal of hand surgery, European volume 39, 263–271. [PubMed: 23697681]

Tay SC, Primak AN, Fletcher JG, Schmidt B, Amrami KK, Berger RA, McCollough CH, 2007. Four-dimensional computed tomographic imaging in the wrist: proof of feasibility in a cadaveric model. Skeletal radiology 36, 1163–1169. [PubMed: 17805530]

Tay SC, Primak AN, Fletcher JG, Schmidt B, An KN, McCollough CH, 2008. Understanding the relationship between image quality and motion velocity in gated computed tomography: preliminary work for 4-dimensional musculoskeletal imaging. J Comput Assist Tomogr 32, 634–639. [PubMed: 18664854]

Thévenaz P, Blu T, Unser M, 2008. Image Interpolation and Resampling, in: Bankman I (Ed.), Handbook of Medical Image Processing and Analysis, 2 ed. Elsevier, pp. 465–494.

Trentadue TP, Lopez C, Breighner RE, Fautsch K, Leng S, Holmes DR Iii, Moran SL, Thoreson AR, Kakar S, Zhao KD, 2023. Evaluation of scapholunate injury and repair with dynamic (4D) CT: a preliminary report of two cases. J Wrist Surg.

Viegas SF, Yamaguchi S, Boyd NL, Patterson RM, 1999. The dorsal ligaments of the wrist: anatomy, mechanical properties, and function. The Journal of hand surgery 24, 456–468.

Waters MS, Werner FW, Haddad SF, McGrattan ML, Short WH, 2016. Biomechanical evaluation of scaphoid and lunate kinematics following selective sectioning of portions of the scapholunate interosseous ligament. The Journal of hand surgery 41, 208–213. [PubMed: 26718075]

Watson HK, Ballet FL, 1984. The SLAC wrist: scapholunate advanced collapse pattern of degenerative arthritis. The Journal of hand surgery 9, 358–365. [PubMed: 6725894]

Watson HK, Weinzweig J, Zeppieri J, 1997. The natural progression of scaphoid instability. Hand clinics 13, 39–49. [PubMed: 9048182]

White J, Couzens G, Jeffery C, 2019. The use of 4D-CT in assessing wrist kinematics and pathology: a narrative view. Bone Joint J 101-b, 1325–1330. [PubMed: 31674237]

Wu G, van der Helm FC, Veeger HE, Makhsous M, Van Roy P, Anglin C, Nagels J, Karduna AR, McQuade K, Wang X, Werner FW, Buchholz B, 2005. ISB recommendation on definitions of joint

coordinate systems of various joints for the reporting of human joint motion--Part II: shoulder, elbow, wrist and hand. Journal of biomechanics 38, 981–992. [PubMed: 15844264]

Zhao K, Breighner R, Holmes D 3rd, Leng S, McCollough C, An KN, 2015. A technique for quantifying wrist motion using four-dimensional computed tomography: approach and validation. J Biomech Eng 137, 0745011–0745015. [PubMed: 25901447]

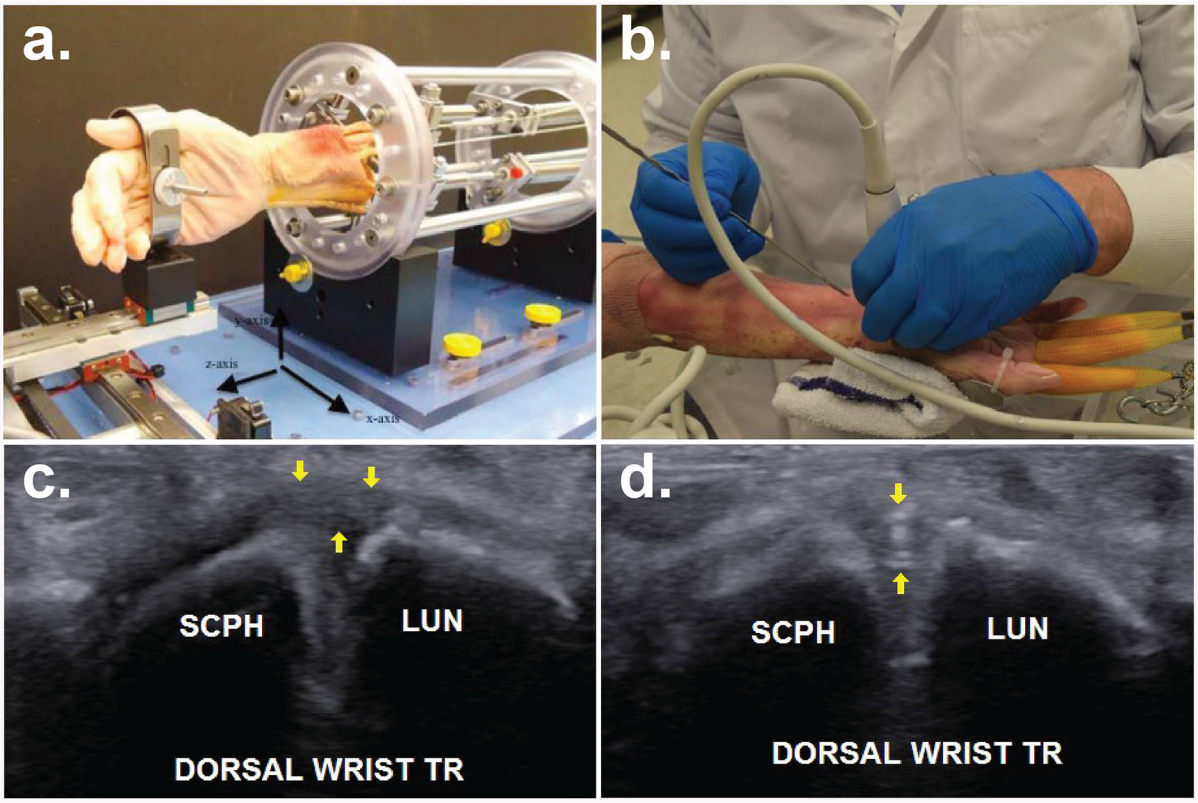

Figure 1:
Cadaveric specimen preparation and motion simulation. (a) Cadaver forearm and wrist positioning within the motion simulator and (b) experimental set-up for ultrasound-guided ligament sectioning. Validation image demonstrating the dorsal scapholunate interosseous ligament (DSL) under ultrasound (c) intact and (d) while being sectioned. In (c), the DSL is highlighted between three yellow arrows. In (d), the vertically-oriented meniscotome is placed perpendicular to the DSL in preparation for ligament sectioning, with the yellow arrows indicating hyperechoic metal artifact from the meniscotome. DSL = dorsal scapholunate interosseous ligament; LUN = lunate; SCPH = scaphoid.

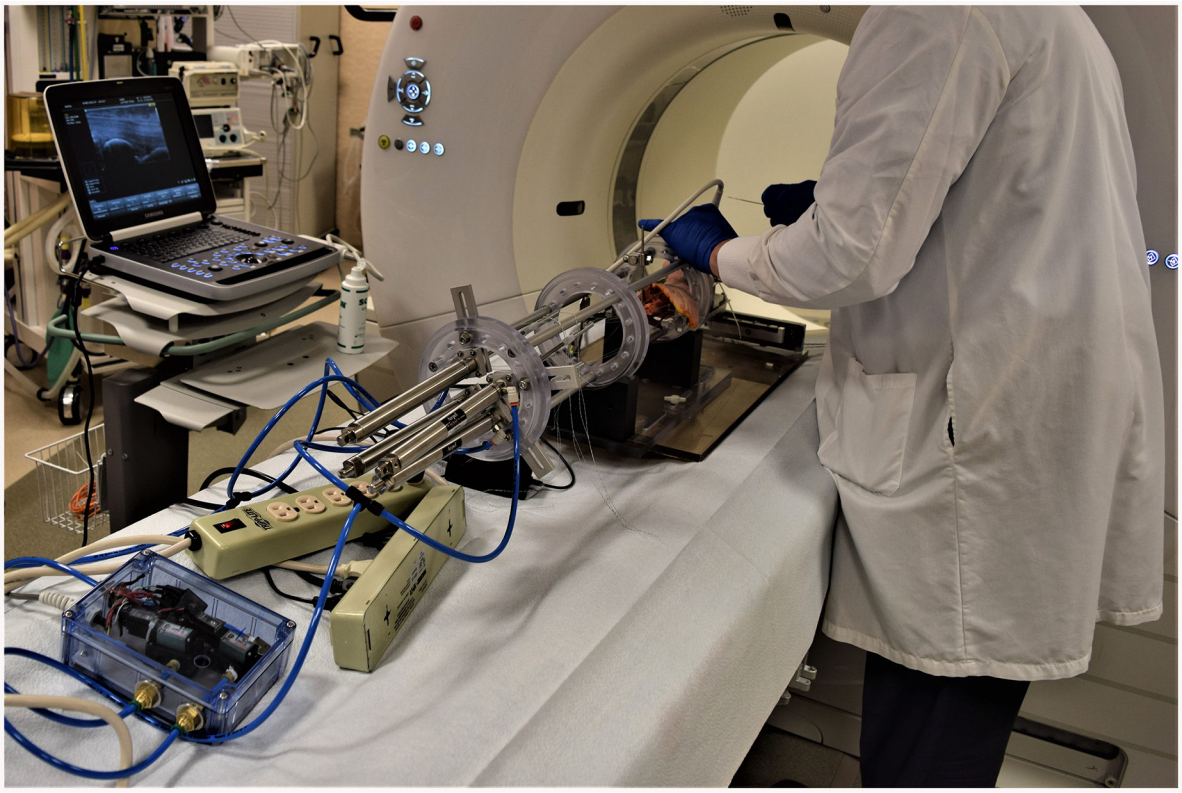

Figure 2:
Photograph of the CT imaging suite containing the cadaveric forearm and hand mounted within the pneumatic cylinder-driven wrist simulator, ultrasound system for image-guided ligamentous sectioning, and position of the apparatus on the CT table relative to the CT gantry.

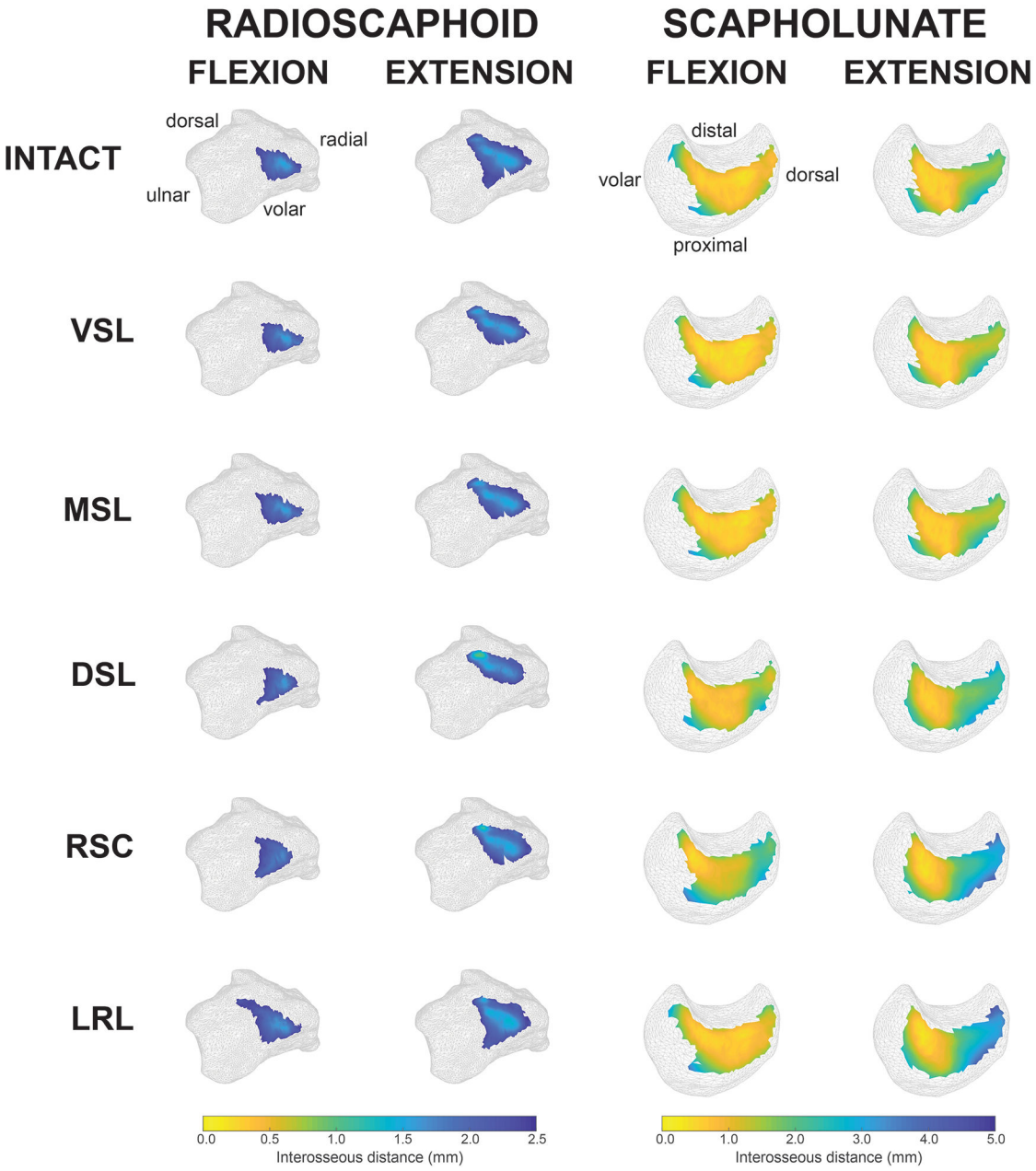

Figure 3:

Demonstrative proximity maps at the extrema of flexion-extension at the radioscaphoid joint (RS) and scapholunate interval (SL) presented on the distal radius and radial lunate, respectively, across ligament integrity conditions following sequential ligamentous injuries (PRE = intact, VSL = volar scapholunate interosseous ligament, MSL = membranous scapholunate interosseous ligament, DSL = dorsal scapholunate interosseous ligament, RSC = radioscaphocapitate ligament, LRL = long radiolunate ligament). Extrema of motion were determined using the maximum and minimum angles between the long axes of the radius and capitate.

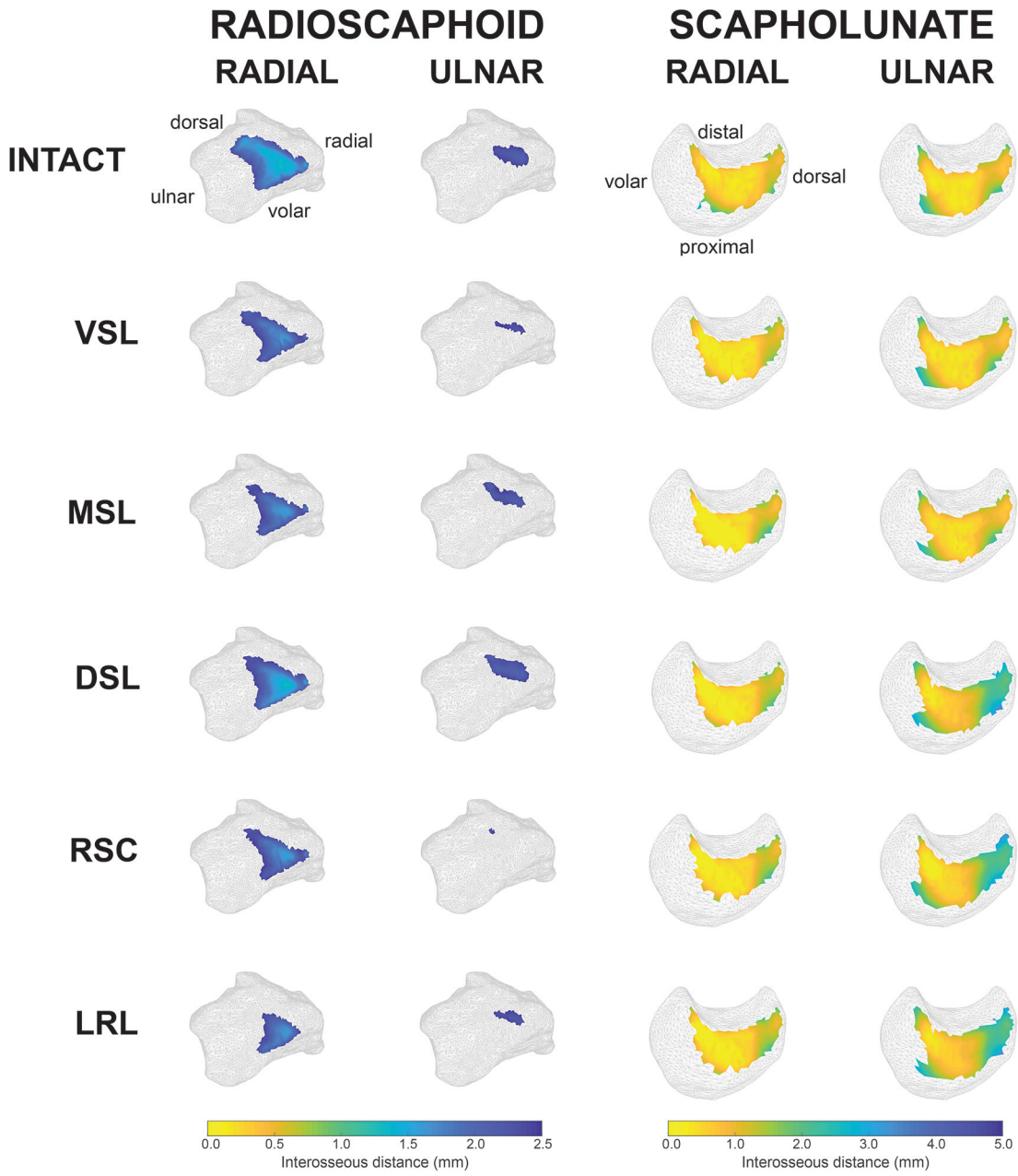

Figure 4:

Demonstrative proximity maps at the extrema radioulnar deviation at the radioscaphoid joint (RS) and scapholunate interval (SL) presented on the distal radius and radial lunate, respectively, across ligament integrity conditions following sequential ligamentous injuries (PRE = intact, VSL = volar scapholunate interosseous ligament, MSL = membranous scapholunate interosseous ligament, DSL = dorsal scapholunate interosseous ligament, RSC = radioscaphocapitate ligament, LRL = long radiolunate ligament). Extrema of motion were determined using the maximum and minimum angles between the long axes of the radius and capitate.

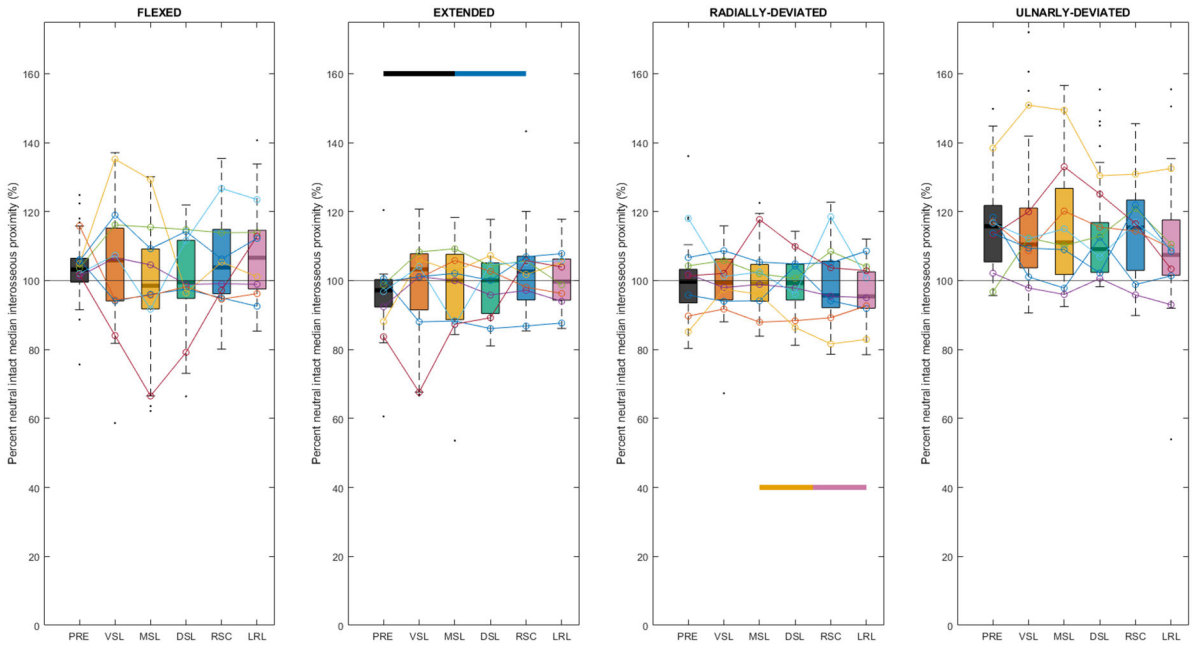

Figure 5:

Distribution of median interosseous proximities at the radioscaphoid joint in positions relative to the neutral wrist for each ligament cut condition following sequential ligamentous injuries (PRE = intact, VSL = volar scapholunate interosseous ligament, MSL = membranous scapholunate interosseous ligament, DSL = dorsal scapholunate interosseous ligament, RSC = radioscaphocapitate ligament, LRL = long radiolunate ligament) from the eight included cadavers. Interosseous proximity data are normalized to the median interosseous proximity of the intact radioscaphoid joint in the neutral position. Statistical significance between each pair of ligaments is represented by a horizontal bar. Horizontal bars at the top of each subplot represent differences relative to the intact wrist. Horizontal bars at the bottom of each subplot represent differences between two injury states (Supplementary Table 6).

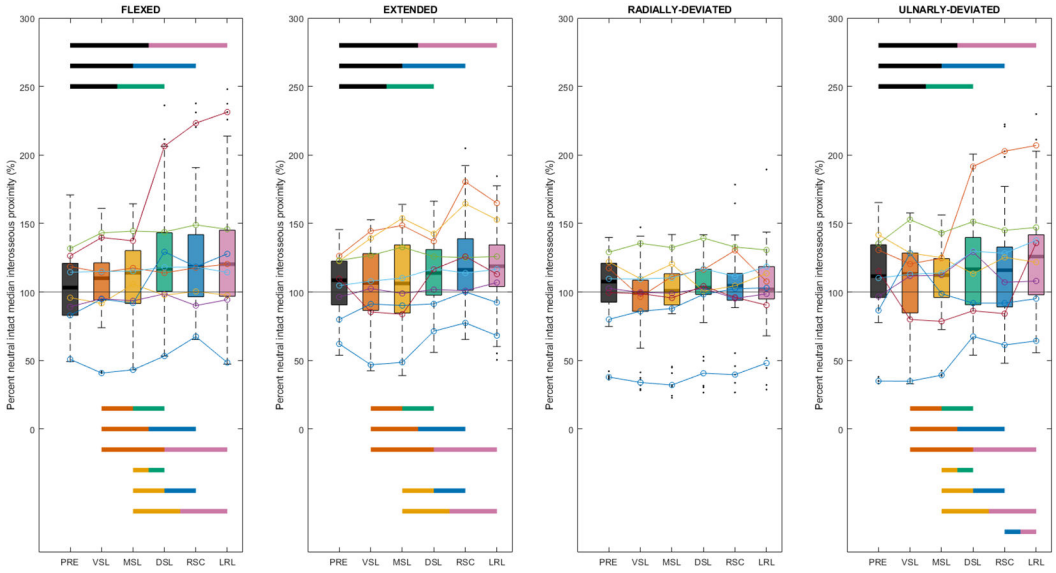

Figure 6:

Distribution of median interosseous proximities at the scapholunate interval in positions relative to the neutral wrist for each ligament cut condition following sequential ligamentous injuries (PRE = intact, VSL = volar scapholunate interosseous ligament, MSL = membranous scapholunate interosseous ligament, DSL = dorsal scapholunate interosseous ligament, RSC = radioscaphocapitate ligament, LRL = long radiolunate ligament) from the eight included cadavers. Interosseous proximity data are normalized to the median interosseous proximity of the intact scapholunate interval in the neutral position. Statistical significance between each pair of ligaments is represented by a horizontal bar. Horizontal bars at the top of each subplot represent differences relative to the intact wrist. Horizontal bars at the bottom of each subplot represent differences between two injury states (Supplementary Table 6).